Dalton Transactions

ROYAL SOCIETY OF CHEMISTRY

COMMUNICATION

View Article Online
View Journal | View Issue

Cite this: *Dalton Trans.*, 2025, **54**, 14648

Received 11th September 2025,
Accepted 19th September 2025

DOI: 10.1039/d5dt02188j

rsc.li/dalton

Structural and electronic tuning of hybrid metal thiocyanate *N*-oxides

Grace M. Robertson and Adam Jaffe *

Hybrid metal thiocyanates are highly tailorable materials isolable under mild synthetic conditions. By varying pyridine-*N*-oxide derivatives within manganese, cobalt, and nickel congeners, we show fine-tuning of structural and electronic features depending on molecular substituent and metal selection, providing a roadmap for application-specific customization and potential property-tuning.

Solid-state materials can offer high chemical and thermal stability, efficient charge transport and storage, and optical absorption in the visible/near-UV[1]—properties that make them suited for wide-ranging applications in solar cells,[2] batteries,[3] sensors,[4] and catalytic systems.[5,6] Despite their favorable qualities, inorganic crystalline compounds often require energy-intensive high-temperature syntheses and have a high kinetic barrier to further modification post-synthesis, giving little room for product fine-tuning. Molecular chemistry, however, is characterized by fine synthetic control with low energy input, though these isolated species lack extended electronic structure and the accompanying desirable optical and electronic properties. Hybrid organic–inorganic materials afford the opportunity to synergistically combine favorable aspects of both molecular and materials chemistry under mild conditions, often with a greater degree of control over important optoelectronic characteristics such as light absorption.

Inorganic metal thiocyanates are an intriguing class of materials to consider as parent compounds for such a hybrid material platform. They often feature wide band gaps and high hole mobilities, making them well-suited for applications in optoelectronic devices.[7–9] Many of these SCN^- materials even exhibit non-linear optical properties such as second-harmonic generation that is relevant for laser technologies.[10,11] Fundamentally, metal thiocyanates' wide-ranging properties arise from the ability to readily incorporate a variety of metal centers as well as a diverse array of metal–thiocyanate coordination modes spanning coordination *via* sulfur and/or nitrogen, as well as bridging—either end-to-end or end-on—or terminal motifs.[12,13] Such chemical and structural tuning allows for significant modification of inorganic metal thiocyanates' electronic structure.

To then greatly enhance the modularity and tunability of metal thiocyanates, organic molecules can be incorporated as ligands within the structure, thereby producing hybrid metal thiocyanates (Fig. 1) as an even more versatile platform. Many reports have examined amine-based ligands,[14–21] however their *N*-oxide counterparts have been less widely studied. The combination of both *N*-oxide and thiocyanate ligands offers a vast structural phase space according to the multiple possible binding and bridging motifs for these species,[12,13] presenting an opportunity to finely tune structural, electronic, and optical characteristics. However, greater insight into hybrid metal thiocyanates is still required.

Amine *N*-oxides such as pyridine-*N*-oxide (pyO) are attractive molecular species from which to construct hybrid materials, owing to their relatively high air and water stability,

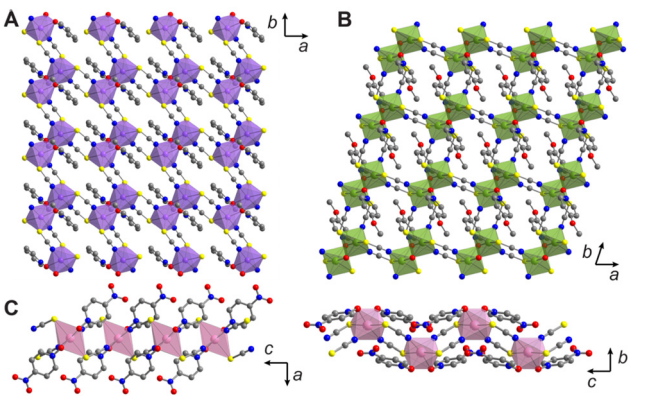

Fig. 1 X-ray structures of 2D (A) $Co(NCS)_2$(2-MepyO) and (B) $Ni(NCS)_2$(4-MeOpyO), and 1D (C) $Mn(NCS)_2(4\text{-}NO_2pyO)_2$ (two views). Gray, blue, red, yellow, purple, green, and pink spheres are C, N, O, S, Co, Ni, and Mn, respectively. Polyhedra show connectivity.

Department of Chemistry and Biochemistry, University of Notre Dame, Notre Dame, Indiana 46556, USA. E-mail: ajaffe@nd.edu

their versatile binding behavior as relatively weak ligands, and their robust set of derivatives based on pyridyl ring substituent(s).[22,23] Indeed, the position of these substituents can direct metal coordination as a function of steric, electronic, and other intermolecular interactions. Despite the relatively low pK_a of the conjugate acid for pyO (0.79) compared with that of pyridine (5.18),[24] hybrid materials containing pyO-based ligands have been reported that incorporate metals such as Co, Ni, Mn, Zn, and Cd, as well as bridging pseudohalides such as thiocyanates or azides.[25–33] However, many of these reports focus on just one or two compounds within the much larger potential material family, and furthermore, relationships between structural and electronic properties remain underexplored. Ultimately, these extended structures offer potential as compounds that may find their place in key applications listed above model systems as well as systems from which to derive key fundamental insight and material design principles based on how metal–ligand combinations dictate symmetry, binding modes, connectivity, and emergent electronic behavior.

Here, we examine pyO-based metal thiocyanate hybrids (Fig. 1) by interrogating how the selection of transition metal center and pyO derivative translates to structural modulation and resultant optical and electronic behavior. In this work, we survey hybrid materials based on Mn, Ni, and Co and incorporate four pyridine-*N*-oxide molecules: 2-MepyO (Me = methyl), 4-MepyO, 4-MeOpyO (MeO = methoxy), and 4-NO_2pyO. We report five new compounds within this material family and show that the *N*-oxide used in the synthesis directs the overall structure of the solid as well as the electronic transitions that are observed. While the metal does not greatly influence the overall connectivity of the structure, it does manifest subtle structural differences that relate to periodic trends and further tunes the energy of electronic transitions.

Metal thiocyanate hybrids of the formula $M(NCS)_2(L)_z$ (L = pyO-based ligand, M = metal; z = 1 or 2) were synthesized under aerobic conditions by combining the appropriate metal nitrate, *N*-oxide, and potassium thiocyanate in either water or methanol. Single crystals suitable for structure determination of $Co(NCS)_2$(2-MepyO), $Ni(NCS)_2$(2-MepyO), $Ni(NCS)_2$(4-MeOpyO), $Ni(NCS)_2$(4-NO_2pyO)$_2$, and $Mn(NCS)_2$(4-NO_2pyO)$_2$ (Tables S1 and S2) as well as powder samples for other compounds were obtained through a slow evaporation method (see SI for synthetic procedures). Powder X-ray diffraction patterns demonstrate that Mn, Co, and Ni analogs are isostructural, given a particular *N*-oxide species, even in cases where single crystals were not achieved such as $Mn(NCS)_2$(4-MepyO) and $Mn(NCS)_2$(4-MeOpyO) (Fig. S1–S4). As previously stated, we report five new hybrid metal thiocyanates: $Mn(NCS)_2$(4-MepyO), $Mn(NCS)_2$(4-MeOpyO), $Ni(NCS)_2$(4-MeOpyO), $Ni(NCS)_2$(2-MepyO), and $Ni(NCS)_2$(4-NO_2pyO)$_2$. We have completed the matrix of compounds in Table 1,[25–31] allowing us to systematically evaluate the effects of metal and ligand.

In the cases of 2-MepyO, 4-MepyO, and 4-MeOpyO, all metals (Mn, Co, and Ni) result in a two-dimensional structure of the formula $M(NCS)_2(L)$ as shown in Fig. 1A and B. Here, each 2D sheet is comprised of six-coordinate octahedral metal centers (Fig. S5) where ligand choice dictates the metal coordination sphere. When employing 4-MepyO and 4-MeOpyO ligands, each of the ligand pairs—thiocyanate N atoms, thiocyanate S atoms, and pyO oxygen atoms—are oriented in *cis* conformations. In 2-MepyO structures, the O atoms are *cis* as are the S atoms, but the pair of N atoms are *trans*. The extended framework structure features metal centers bridged in a μ_2 fashion through the oxygen atom of the *N*-oxide ligand as well as μ_2-bridged in an end-to-end fashion through the sulfur and nitrogen of the SCN^-. The 2D layers within these compounds contain pockets that partially accommodate the organic ligands that also extend into the interlayer space—the *para*-substituted molecules more so than the *ortho*-substituted case. Interestingly the 4-NO_2pyO materials form a 1D structure with either Mn, Co, or Ni and a general formula of $M(NCS)_2(L)_2$, where SCN^- bridges the metal centers in a non-linear, end-to-end "zigzag" arrangement which can be seen when viewing the structure along the *a* axis (Fig. 1C). In contrast to the 2D structures, the 4-NO_2pyO ligands are bound terminally to the metal center—yielding the new $M(NCS)_2(L)_2$ formula with two pyO ligands per metal center—likely due to a combination of steric hindrance from the bulkier nitro substituent on the pyridine ring, and electronic effects due to its electron withdrawing and resonance behavior (see discussion below). Another notable feature of this set of 1D structures is that the *N*-oxide ligands bound to each metal center occupy positions alternating above and below the metal centers when observed along the *b* axis (Fig. 1C), which accommodates the 1D zigzag geometry of the metal–thiocyanate chain. The metal coordination is similar to that of the 2-MepyO case, however here the S atoms are *trans* and the N atoms are *cis*. Structural comparison across the material family also reveals that manganese yields the longest metal–ligand bonds, while nickel exhibits the shortest, irrespective of *N*-oxide ligand (Tables S3 and S4). This trend agrees with expectations based on metal ion atomic radius and effective nuclear charge, Z_{eff}.

Vibrational characterization reveals intense bands at approximately 2100 cm^{-1} in both infrared (IR) absorption and Raman spectra (Fig. 2 and S6, S7), corroborating prior literature reports for thiocyanate CN stretching modes.[26,28–31] Here, Ni compounds display the highest frequency CN stretches, followed by Co, then Mn, which is consistent with their electronegativities, producing increasing backbonding from the metal to thiocyanate π^* orbitals across this series. Electrostatics may

Table 1 $M(NCS)_2(L)_z$ (L = pyO derivative; z = 1 or 2) structural family

	Mn	Co	Ni
2-MepyO	Reported[28]	Reported[25 b]	This work
4-MepyO	This work[a]	Reported[29]	Reported[30]
4-MeOpyO	This work[a]	Reported[31]	This work
4-NO_2pyO	Reported[27 b]	Reported[26]	This work

[a] Powder diffraction data only. [b] Structures that were recollected in this work.

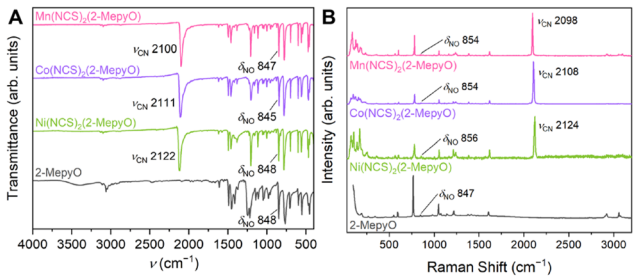

Fig. 2 (A) IR and (B) Raman spectra for $M(NCS)_2$(2-MepyO) where M = Co, Ni, and Mn.

also play a role in this trend: increased charge density and electronegativity can enhance electron density withdrawal from the thiocyanate and strengthen the C–N bond, raising the stretching frequency as a function of metal ion.[34,35] Vibrational peaks are also observed at *ca.* 850 cm^{-1}, which we assign as N–O bending modes of the pyO derivatives.[36] We note that these peaks are not appreciably shifted relative to their values observed for the molecular solids.

To probe the electronic properties of these materials more directly, we performed UV-visible diffuse reflectance spectroscopy (UV-vis) measurements, benchmarking the hybrid metal thiocyanates against *N*-oxide molecules (Fig. 3). While reports of magnetic behavior for hybrid metal pseudohalides are numerous,[26,28,30] their electronic absorption behavior is less well-studied. We attribute low-intensity peaks below *ca.* 3 eV to d–d transitions. These weak bands are observed for Co and Ni, and to a much lesser extent in the case of Mn, in agreement with a high-spin d^5 electronic configuration for Mn that would make these already Laporte-forbidden transitions also spin-forbidden. This low-intensity feature *ca.* 2.2 eV for the Mn solids—excluding the 4-NO_2pyO-based compound that exhibits an intense lower-energy charge-transfer band that obscures the weak feature—is likely attributable to the ligand field splitting of the $^6A_1$ ground state (Fig. S8). Meanwhile, the Co and Ni d–d transitions track well with those expected for six-coordinate weak-field complexes according to their corresponding Tanabe–Sugano diagrams for d^7 and d^8 centers, respectively.[37] Here, we extracted ligand field parameters for $Co(NCS)_2$(2-MepyO) and $Ni(NCS)_2$(2-MepyO) (Tables S5 and S6) as representative materials—as seen in Fig. 4, materials based on the same metal display similar d–d peak positions regardless of ligand. In the case of Ni, ligand field analysis yields a Racah parameter of B = 770 ± 9 cm^{-1} and a ligand field splitting of Δ_O = 8773 ± 104 cm^{-1}. Considering the free-ion value of Ni^{2+},[37] β was determined to be 0.75, consistent with moderate metal–ligand covalency as described by the nephelauxetic effect. In comparison, Co has a noticeably smaller B value of 587 ± 13 cm^{-1} with β = 0.60 and larger Δ_O of 9739 ± 219 cm^{-1}. This shift in the ligand field parameters indicates both greater metal–ligand covalency and stronger ligand field stabilization in the case of Co.

Two bands originating from the pyO derivatives are present in the diffuse reflectance spectra of molecular *N*-oxides, as well as the hybrid materials. In the case of 2-MepyO, 4-MepyO, and 4-MeOpyO these partially overlapping bands appear above 3.6 eV (Fig. 3A–C) and we assign them as likely arising from intra-ligand transitions from non-bonding (n.b.) O 2p-derived orbitals to the pyO π^* state as well as from the pyO π to π^*.[36] The lower absorption onset *ca.* 3.1 eV for 4-NO_2pyO (Fig. 3D) is consistent with the electron-withdrawing character of the nitro substituent and its resonance, stabilizing π^*.[38]

Examining electronic transitions unique to the hybrid solids, when considering the 2-MepyO, 4-MepyO, and 4-MeOpyO materials, intense absorption is observed from 2.5–3.5 eV (Fig. 3, 4 and Table S7). We assign this absorption as predominantly (1) ligand-to-metal-charge-transfer (LMCT) transitions from states primarily derived from thiocyanate sulfur p orbitals to metal d orbitals, in agreement with investigations of inorganic metal thiocyanates;[39,40] and (2) metal-to-ligand-charge-transfer (MLCT) transitions from orbitals dominated by metal d character to the π^* states of ligands.[38] Though subtle, metal substitution tunes the absorption edge onset values (E_M, Fig. S9): $E_{Ni} < E_{Co} \approx E_{Mn}$. However, the combined behavior of both the LMCT and MLCT as a function of metal is complex when considering metal d orbital energies[41] compared to the spectrochemical series of metal ions (σ interactions only),[42] where Mn^{2+} features the least ligand field splitting with less severe σ^* antibonding destabilization of its e_g orbitals when compared to Ni^{2+} and Co^{2+}. Another

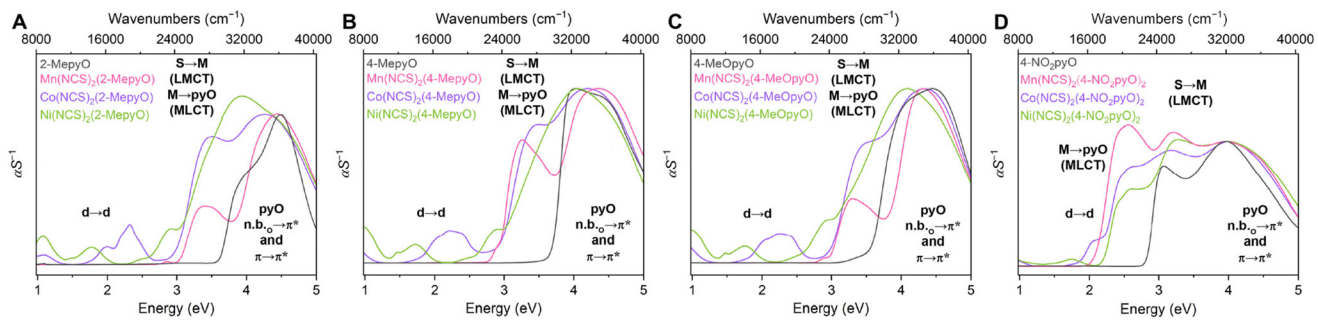

Fig. 3 UV-visible diffuse reflectance spectra as a function of metal for hybrid materials containing (A) 2-MepyO, (B) 4-MepyO, (C) 4-MeOpyO, and (D) 4-NO_2pyO.

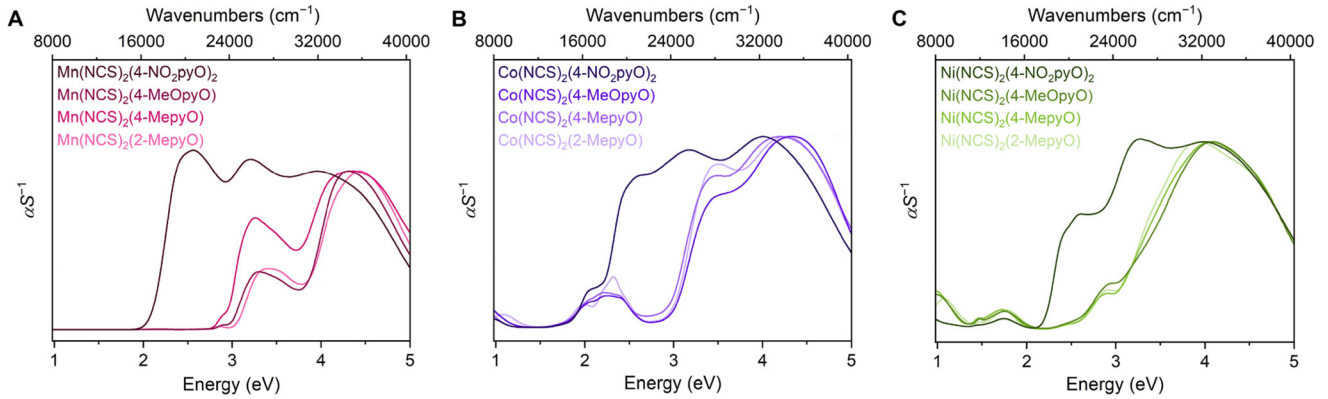

Fig. 4 UV-visible diffuse reflectance spectra of hybrid *N*-oxide materials based on (A) Mn, (B) Co, and (C) Ni.

counterbalancing factor is that the degree of metal electrostatic effects and/or backbonding follows the trend Mn > Co > Ni, according to our IR absorption analysis. Greater backbonding implies greater π stabilization within the t_{2g} orbitals. Also, Mn^{2+} and Co^{2+} are d^5 and d^7 ions, respectively, meaning LMCT transitions are possible to either e_g or t_{2g} states (assuming high-spin), while Ni^{2+} is d^8, leaving the lower-energy d-derived orbitals filled. Thus, the combination of multiple effects on these multiple transitions is challenging to parse. In contrast, for hybrids containing 4-NO_2pyO, a new low-energy absorption feature is observed near 2 eV. These absorption edges are likely MLCT transitions from orbitals with majority metal d character to π^* states of the pyO derivative that are heavily stabilized by the electron-withdrawal and resonance of the nitro substituents. Here, a clear trend is subsequently observed in the absorption edge as a function of metal from 2.10(1) eV for Mn to 2.15(1) eV for Co and 2.20(1) eV for Ni (Fig. 3D, 4 and Table S7). This behavior is consistent with the periodic trend in metal d orbital energies discussed above. Ultimately, the system's modularity in metal, ligand, and structural motif allows for significant tuning of the absorption characteristics critical for future optics and energy applications.

Conclusion

Herein, we have expanded the known phase-space of hybrid metal thiocyanate materials containing pyridine *N*-oxide derivatives by demonstrating systematic fine tuning of structural, vibrational, and electronic parameters. We have shown that the steric bulk of ligands' aryl substituents can influence dimensionality and coordination isomerism, and that metal centers can be readily substituted to yield isostructural compounds while simultaneously tuning the electronic properties of these materials: (1) apparent metal-to-ligand backbonding and electrostatic effects scale with the expected periodic trend for first-row transition metals, (2) the Co congener likely features greater ligand field stabilization and metal–ligand covalency relative to the Ni analog, (3) strong absorption associated with LMCT transitions (thiocyanate sulfur to metal d orbitals) and MLCT transitions (metal d to pyO-derivative π^* orbitals) features a complex dependence on metal d orbital energy, modified by σ and π bonding, and (4) the onset energy of the MLCT transitions can be substantially decreased with electron-withdrawing aryl substituents. This work therefore helps establish design principles for these versatile hybrid metal thiocyanate materials, whose properties can be tuned based on judicious selection of metal–ligand combination. One especially interesting future direction to consider is leveraging atom transfer/exchange chemistry[43–48]—in which molecular reagents feature built-in enthalpic and/or entropic driving forces to install or remove specific atoms—within these or similar hybrid materials while in the solid-state, given amine *N*-oxides' wide exploration as oxygen atom transfer reagents.[22,45,46] By introducing redox-active metal centers with higher reduction potentials and tuning the strength of the N–O bond through the substitution of aryl functional groups,[22] these hybrid materials represent potential key intermediates toward stimulus-driven atom transfer reactions to modify the chemical and electronic properties of the resulting solid-state materials.

Conflicts of interest

There are no conflicts to declare.

Data availability

Supplementary information: experimental details, diffraction patterns, spectra, and supplemental discussion. See DOI: **https://doi.org/10.1039/d5dt02188j**.

CCDC 2468137, 2468212, 2468213, 2468223 and 2468441 ([Ni(NCS)$_2$(4-MeOpyO), Mn(NCS)$_2$(4-NO$_2$pyO)$_2$, Co(NCS)$_2$(2-MepyO), Ni(NCS)$_2$(2-MepyO) and Ni(NCS)$_2$(4-NO$_2$pyO)$_2$) contain the supplementary crystallographic data for this paper.[49a–e]

Acknowledgements

Acknowledgement is made to the donors of the American Chemical Society Petroleum Research Fund for partial support of this research through PRF# 65120-DNI10. We thank ND Energy for support of G. M. R. through the John and Karla Forgash Graduate Student Fellowship for Energy Storage Research and the University of Notre Dame through the Arthur J. Schmitt Presidential Leadership Fellowship. X-ray diffraction studies were carried out at the Notre Dame Molecular Structure Facility. We thank the ND Energy Materials Characterization Facility (MCF) for the use of the UV-Visible spectrometer to acquire diffuse reflectance measurements. The MCF is supported by Notre Dame Research. We thank Dr Allen Oliver for assistance with X-ray diffraction studies.

References

1 A. R. West, *Solid state chemistry and its applications*, John Wiley & Sons, Chichester, West Sussex, U.K., 2014.
2 S. S. Shin, S. J. Lee and S. I. Seok, *Adv. Funct. Mater.*, 2019, **29**, 1900455.
3 M. V. Reddy, G. V. Subba Rao and B. V. R. Chowdari, *Chem. Rev.*, 2013, **113**, 5364–5457.
4 E. Gagaoudakis, V. Kampitakis, M. Moschogiannaki, A. Sfakianou, T. Anthopoulos, L. Tsetseris, G. Kiriakidis, G. Deligeorgis, F. Iacovella and V. Binas, *Sens. Actuators, A*, 2022, **338**, 113462.
5 T. Tan, W. Wang, K. Zhang, Z. Zhan, W. Deng, Q. Zhang and Y. Wang, *ChemSusChem*, 2022, **15**, e202200522.
6 D. Kato, H. Suzuki, R. Abe and H. Kageyama, *Chem. Sci.*, 2024, **15**, 11719–11736.
7 C. Wechwithayakhlung, D. M. Packwood, J. Chaopaknam, P. Worakajit, S. Ittisanronnachai, N. Chanlek, V. Promarak, K. Kongpatpanich, D. J. Harding and P. Pattanasattayavong, *J. Mater. Chem. C*, 2019, **7**, 3452–3462.
8 J. E. Jaffe, T. C. Kaspar, T. C. Droubay, T. Varga, M. E. Bowden and G. J. Exarhos, *J. Phys. Chem. C*, 2010, **114**, 9111–9117.
9 P. Pattanasattayavong, V. Promarak and T. D. Anthopoulos, *Adv. Electron. Mater.*, 2017, **3**, 1600378.
10 D. Yuan, D. Xu, M. Liu, F. Qi, W. Yu, W. Hou, Y. Bing, S. Sun and M. Jiang, *Appl. Phys. Lett.*, 1997, **70**, 544–546.
11 H. Zhang, X. Jiang, Y. Zhang, K. Duanmu, C. Wu, Z. Lin, J. Xu, J. Yang, Z. Huang, M. G. Humphrey and C. Zhang, *J. Am. Chem. Soc.*, 2024, **146**, 28329–28338.
12 E. Shurdha, S. H. Lapidus, P. W. Stephens, C. E. Moore, A. L. Rheingold and J. S. Miller, *Inorg. Chem.*, 2012, **51**, 9655–9665.
13 M. J. Cliffe, *Inorg. Chem.*, 2024, **63**, 13137–13156.
14 J. Songkerdthong, T. Thanasarnsurapong, A. Boonchun, D. J. Harding and P. Pattanasattayavong, *Mol. Syst. Des. Eng.*, 2024, **9**, 814–825.
15 P. Pattanasattayavong, D. M. Packwood and D. J. Harding, *J. Mater. Chem. C*, 2019, **7**, 12907–12917.
16 L. F. Larkworthy and B. J. Tucker, *Inorg. Chim. Acta*, 1979, **33**, 167–170.
17 S. Kisslinger, H. Kelm, S. Zheng, A. Beitat, C. Würtele, R. Wortmann, S. Bonnet, S. Herres-Pawlis, H.-J. Krüger and S. Schindler, *Z. Anorg. Allg. Chem.*, 2012, **638**, 2069–2077.
18 K. M. Miller, S. M. McCullough, E. A. Lepekhina, I. J. Thibau, R. D. Pike, X. Li, J. P. Killarney and H. H. Patterson, *Inorg. Chem.*, 2011, **50**, 7239–7249.
19 C. Näther and J. Boeckmann, *Acta Crystallogr., Sect. E: Struct. Rep. Online*, 2025, **81**, 58–62.
20 C. Näther and J. Boeckmann, *Acta Crystallogr., Sect. E: Struct. Rep. Online*, 2025, **81**, 420–424.
21 C. Näther and A. Jochim, *Acta Crystallogr., Sect. E: Struct. Rep. Online*, 2024, **80**, 677–681.
22 W. E. Acree Jr., G. Pilcher and M. D. M. C. Ribeiro da Silva, *J. Phys. Chem. Ref. Data*, 2005, **34**, 553–572.
23 D. W. Herlocker, R. S. Drago and V. I. Meek, *Inorg. Chem.*, 1966, **5**, 2009–2015.
24 P. Mech, M. Bogunia, A. Nowacki and M. Makowski, *J. Phys. Chem. A*, 2020, **124**, 538–551.
25 C. Näther and I. Jess, *Acta Crystallogr., Sect. E: Struct. Rep. Online*, 2024, **80**, 67–71.
26 J.-M. Shi, J.-N. Chen, C.-J. Wu and J.-P. Ma, *J. Coord. Chem.*, 2007, **60**, 2009–2013.
27 J. Shi, J. Chen and L. Liu, *Pol. J. Chem.*, 2006, **80**, 1909–1913.
28 F. A. Mautner, C. Berger, R. C. Fischer, S. S. Massoud and R. Vicente, *Polyhedron*, 2018, **141**, 17–24.
29 S.-G. Zhang, W.-N. Li and J.-M. Shi, *Acta Crystallogr., Sect. E: Struct. Rep. Online*, 2006, **62**, 3506–3608.
30 J.-M. Shi, Y.-M. Sun, Z. Liu and L.-D. Liu, *Chem. Phys. Lett.*, 2006, **418**, 84–89.
31 S.-G. Zhang, W.-N. Li and J.-M. Shi, *Acta Crystallogr., Sect. E: Struct. Rep. Online*, 2006, **62**, 3398–3400.
32 F. A. Mautner, C. Berger, R. C. Fischer and S. S. Massoud, *Inorg. Chim. Acta*, 2016, **448**, 34–41.
33 F. A. Mautner, C. Berger, R. C. Fischer, S. S. Massoud and R. Vicente, *Polyhedron*, 2017, **134**, 126–134.
34 A. S. Goldman and K. Krogh-Jespersen, *J. Am. Chem. Soc.*, 1996, **118**, 12159–12166.
35 N. Roig, R. Van Lommel, M. Alonso and A. B. Chaplin, *Organometallics*, 2024, **43**, 2787–2796.
36 N. M. Karayannis, L. L. Pytlewski and C. M. Mikulski, *Coord. Chem. Rev.*, 1973, **11**, 93–159.
37 Y. Tanabe and S. Sugano, *J. Phys. Soc. Jpn.*, 1954, **9**, 766–779.
38 W. Byers, B. F.-C. Chou, A. B. P. Lever and R. V. Parish, *J. Am. Chem. Soc.*, 1969, **91**, 1329–1333.
39 E. N. Bassey, J. A. M. Paddison, E. N. Keyzer, J. Lee, P. Manuel, I. da Silva, S. E. Dutton, C. P. Grey and M. J. Cliffe, *Inorg. Chem.*, 2020, **59**, 11627–11639.
40 M. J. Cliffe, E. N. Keyzer, M. T. Dunstan, S. Ahmad, M. F. L. De Volder, F. Deschler, A. J. Morris and C. P. Grey, *Chem. Sci.*, 2019, **10**, 793–801.
41 J. B. Mann, T. L. Meek, E. T. Knight, J. F. Capitani and L. C. Allen, *J. Am. Chem. Soc.*, 2000, **122**, 5132–5137.
42 T. Ishii, S. Tsuboi, G. Sakane, M. Yamashita and B. K. Breedlove, *Dalton Trans.*, 2009, **4**, 680–687.

43 L. K. Woo, *Chem. Rev.*, 1993, **93**, 1125–1136.
44 R. H. Holm, *Chem. Rev.*, 1987, **87**, 1401–1449.
45 I. Habib, K. Singha and M. Hossain, *ChemistrySelect*, 2023, **8**, e202204099.
46 A. Petrosyan, R. Hauptmann and J. Pospech, *Eur. J. Org. Chem.*, 2018, 5237–5252.
47 R. H. Holm, *Coord. Chem. Rev.*, 1990, **100**, 183–221.
48 T. Kojima, K. Nakayama, M. Sakaguchi, T. Ogura, K. Ohkubo and S. Fukuzumi, *J. Am. Chem. Soc.*, 2011, **133**, 17901–17911.
49 (*a*) CCDC 2468137: Experimental Crystal Structure Determination, 2025, DOI: **10.5517/ccdc.csd.cc2nv9b5**; (*b*) CCDC 2468212: Experimental Crystal Structure Determination, 2025, DOI: **10.5517/ccdc.csd.cc2nvcrn**; (*c*) CCDC 2468213: Experimental Crystal Structure Determination, 2025, DOI: **10.5517/ccdc.csd.cc2nvcsp**; (*d*) CCDC 2468223: Experimental Crystal Structure Determination, 2025, DOI: **10.5517/ccdc.csd.cc2nvd31**; (*e*) CCDC 2468441: Experimental Crystal Structure Determination, 2025, DOI: **10.5517/ccdc.csd.cc2nvm49**.